Borys Bednarek, Rafał Jurkiewicz, Agnieszka Rzeźnikiewicz

Detectability of Welding Imperfections in Non-Destructive PA and TOFD Ultrasonic Tests

Abstract: The primary objective of the article was to compare the PA and TOFD ultrasonic technique-based detectability of internal imperfections in welded joints. The scope of tests involved the making of joints as well as the performance of ultrasonic, radiographic and macroscopic metallographic tests. The tests enabled the comparison of indications obtained in the tests with the actual location and the size of imperfections. The test results were then compared to identify the accuracy of each technique in relation to previously assumed measurement requirements (e.g. the depth at which a given imperfection was located, characteristic dimensions, offset from the weld axis, etc.).

Keywords: non-destructive tests, visual tests, ultrasonic tests, radiographic tests, PA, TOFD, welding imperfections, boiler steel P265GH

DOI: *10.17729/ebis.2022.1/2*

Introduction

The dynamic diversification of welding technologies over the past few decades has resulted in the popularisation of welding processes in various industries. Owing to their fabrication methods, properties and applications, welded joints are now present in numerous structures and machines exposed to various conditions and loads. The foregoing has entailed the introduction of rigorous weld quality-related requirements. Both the manufacturer and the purchaser must be certain that a specific weld will successfully transfer a predefined load in a given, often unfavourable, work environment. In terms of quality assessment, an important issue is concerned with volumetric tests of welded joints.

One of the solutions to the above-presented problem involves the use of an ultrasonic method, making it possible to test joints having thicknesses of tens of millimetres. Particular attention should be paid to two ultrasonic testing techniques, i.e. the Phased Array (PA) and the Time-of-Flight Diffraction (TOFD) methods. The comparison of indication accuracy could prove useful when analysing and comparing the efficacy the above-named techniques with other methods used to detect internal imperfections [1,2].

Volumetric tests of welded joints

Welding imperfections could be present both on the surface as well as in internal layers of joints. Therefore, the highest efficacy can be

inż. Borys Bednarek, mgr Rafał Jurkiewicz – Łukasiewicz Research Network – Instytut Spawalnictwa, Research Group for Non-Destructive Testing; dr inż. Agnieszka Rzeźnikiewicz – Silesian University of Technology, Faculty of Mechanical Engineering

achieved using combined non-destructive methods involving both surface and volumetric tests. The most important techniques of the latter group include ultrasonic and radiographic tests. In spite of similar methodology, both techniques differ both in terms of their mechanism and properties and, consequently, preferable applications. The knowledge of related values is of key importance as regards industrial implementations of testing methods. The short characteristic and comparison of the aforesaid techniques are presented in Table 1.

It should be taken into consideration that the above-presented values result from averaging, simplifications and standard determinations and may significantly differ from the actual state. An example of the aforesaid phenomenon could be the range of thicknesses of elements tested by means of ultrasonic methods. In spite of the fact that (in terms of the standard) the aforementioned range is restricted between 8 mm and 100 mm, the TOFD technique enables the analysis of joints having a thickness of 6 mm, whereas the ultrasonic wave can penetrate depths significantly exceeding 100 mm. An identical situation can be observed as regards the qualification of testing personnel as the ease of interpreting oscillograms and radiograms depends primarily on inspector's skills and experience [1,3].

Tests

The tests discussed in the article aimed to compare indications (obtained using selected ultrasonic techniques, i.e. TOFD and PAUT) representing internal discontinuities with results of macroscopic and radiographic tests.

The research required the performance of the following activities:

- making a welded joint,
- testing the welded joint using the radiographic method,
- testing the welded joint using the PAUT (i.e. ultrasonic) method,
- testing the welded joint using the TOFD (i.e. ultrasonic) method,
- preparation of the weld for metallographic tests,
- macroscopic metallographic tests of the welded joint.

Table 1. Selected properties of ultrasonic and radiographic methods [2,3]

Feature	UT	RT
Detectability of flat discontinuities perpendicular to the beam axis	very good	poor
Detectability of flat discontinuities along the beam axis	none	good
Detectability of volumetric discontinuities	good	very good
Range of thicknesses of analysed elements	8–100 mm	up to 80 mm (for steels)
Minimum dimensions of detected imperfections	0.001 mm in width and 0.7 mm in length (flat discontinuities), 0.7 mm in diameter (volumetric discontinuities), 0.1 mm in height	Height restricted within the range of 0.5% to 2% of the thickness (of tested elements) and 0.1 mm in width
Inspection costs	medium	high (2–3 times the cost of UT)
Measurement equipment costs	high	very high
Personnel's qualifications	high	very high
Health hazards	none	X-ray and gamma radiation

Materials

The welded joint subjected to the tests was made of boiler steel P265GH. The dimensions of the plates were 300 mm× 133 mm× 10 mm. The above-named steel is characterised by high temperature and high pressure resistance, favourable weldability and lower strength (resulting from a carbon content). Boiler steel P265GH, popular in the power engineering sector, is used in the fabrication of boilers, boiler pipes and heating system elements [5]. The chemical composition and the properties of the test steel are presented in Tables 2 and 3.

The tests also involved the use of a CARBOFIL Mo filler metal in the form of a solid copper-plated wire. The aforesaid wire is used in the MIG (131) and MAG (135) welding of low-alloy ferritic steels exposed to high temperature [7].

The chemical composition of the filler metal wire and that of the weld deposit are presented in Table 4.

Digital detector

The radiographic tests were performed using the following devices:

– Perkin Elemer XRpad 4336 digital detector,
– Eresco 65 MF3 directional transducer tube.

Perkin Elemer XRpad 4336 (Fig. 1a) is a lightweight cordless digital detector featuring a high-resolution matrix and a CsI simulator, guaranteeing the obtainment of very sharp images using only slight radiation doses. In addition, the small dimensions of the device facilitate its transport and operation during

Fig. 1. Equipment used in the radiographic tests: a) Perkin Elemer XRpad 4336 detector and b) Eresco 65 MF3 transducer tube [9,10]

Table 2. Chemical composition of steel P265GH [6]

Chemical element	C	Si	Mn	P	S	Cr	Mo	Ni	Al	Cu	Nb	Ti
Maximum content, %	0.2	0.4	1.4	0.025	0.02	0.3	0.08	0.3	0.02	0.3	0.01	0.04

Table 3. Mechanical properties of steel P265GH [6]

Tensile strength R_m, MPa[1)]	Conventional yield point $R_{p0.2}$, MPa[1)]	Elongation A, %		Impact energy KV, J [2)]	
		longitudinal	transverse	in the longitudinal direction	in the transverse direction
410÷570	265	23	21	40	27
1) For specimens with the wall thickness t ≤ 16 mm. 2) For specimens tested at 0°C.					

Table 4. Chemical composition of the CARBOFIL Mo wire and of the weld deposit [8]

	Maximum content, %					
	C	Mo	Si	Mn	P	S
Wire	0.1	0.5	0.6	1	0.02	0.02
Weld deposit [1)]	0.1	0.5	0.4	0.8	0.02	0.02
1) shielded by the 82%Ar + 18% CO_2 mixture (in accordance with PN-EN ISO 14175:2009)						

tests. In turn, an **Eresco 65 MF3** tube (Fig. 1b) is a portable generator of X-radiation, capable of X-raying steel elements having a thickness of up to 60 mm. The tube features a built-in real-time clock, significantly increasing testing personnel's and third parties' safety by turning off the generator immediately after the completion of the testing process [9,10].

Ultrasonic defectoscope

The tests involving the use of the TOFD and PAUT methods were performed using an Olympus-made set composed of the following elements:

- OmniScann SX 1664PR PA defectoscope (Fig. 2),
- HST-Lite scanner with ST1-70L-IHS wedges (Fig. 3),
- two TOFD V564-SL 15MHz/3mm transducers (Fig. 3),
- PAUT 5L32-A31 transducers,
- 5682 30 MHz PRE-AMPLIFIER,
- hose supplying the cooling medium to the transducer,
- power supply units and cables.

OmniScan SX 1664PR PA is an advanced digital detector enabling the observation and recording of results obtained in tests performed using "classical" methods, i.e. PAUT and TOFD. The touch screen and the legible interface enable the easy performance of tests and the analysis of their results. The specifications of the defectoscope are presented in Table 5.

Table 5. Specifications of the OmniScan SX 1664PR PA defectoscope [11]

Parameter	Value
Display type	TFT LCD
Display dimensions, mm	213 (diagonal)
Display resolution, px	800×600
Types of scans	sectoral, linear
Refresh rate, Hz	60 (for A-scan and S-scan)
Maximum number of saved programmes	256

The **HST-Lite** scanner is a manually operated device used to maintain the proper position of transducers during scanning. Four magnetic wheels and two holders fixed on springs enable easy movements during tests of flat surfaces, pipes or sections. The scanner was designed having the TOFD technique in mind, yet, owing to the adjustable spacing of individual elements and their easy removal, it can also be used in conventional ultrasonic tests (UT) and in phased-array ultrasonic tests (PAUT). The only limitations of the device are its dimensions (125 mm in length, 385 mm in width and 100 mm in height) and the length of the conduit connecting the scanner with the defectoscope (up to 5 m) [12].

Welded joint

The first stage of the tests involved the making of a welded joint. Elements made of steel P265GH were subjected to V-groove

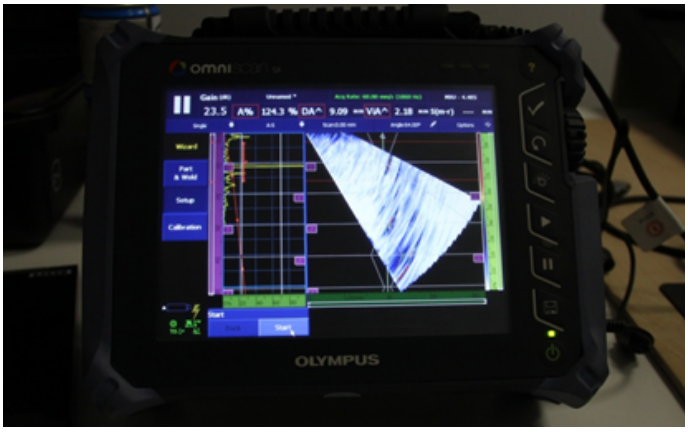

Fig. 2. OmniScan SX during phased-array ultrasonic tests (visible S-scan and A-scan)

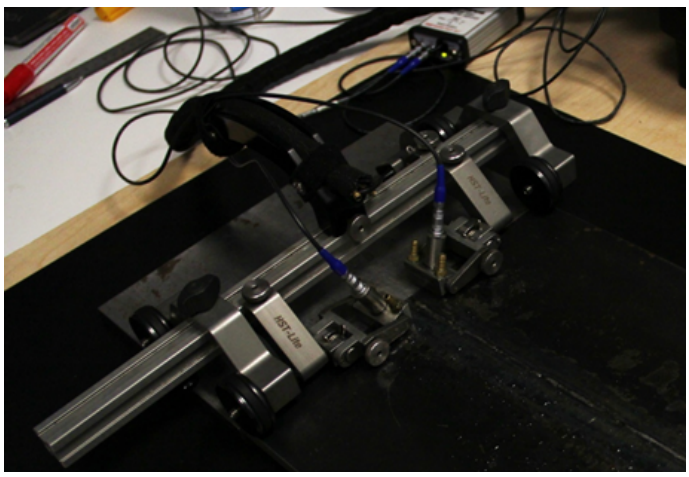

Fig. 3. The HST-Lite scanner with TOFD transducers (pre-amplifier in the background)

preparation, cleaning and, next, welding (process parameters are presented in Table 6). The welded joint was left to cool and, afterwards, was designated in accordance with the NDT terminology (Fig. 4).

Table 6. Welding process parameters

Parameter	Value
Welding method	MAG (135)
Current type and polarity	DC (+)
Electric arc voltage, V	20
Filler metal wire feeding rate, m/min	2,1
Wire diameter, mm	1,2
Welding rate, mm/s	5
Shielding gas	82%Ar+18%CO_2
Gas flow rate, l/min	13

Visual test

The quality of each weld should be verified using visual tests (VT). However, the aforesaid tests are only capable of detecting external discontinuities. As a result, in comparison with volumetric methods, the significance of visual tests is of secondary nature. In addition, there is a risk that a sufficiently high surface imperfection could "eclipse" an imperfection located deeper in the weld and, consequently, lead to the misinterpretation of a radiogram. For this reason, the joint subjected to analysis was tested for the presence of large external imperfections, both on the weld face and weld root side (Fig. 4). The inspection did not reveal the presence of defects which could significantly affect the results of ultrasonic (UT) and radiographic tests (RT).

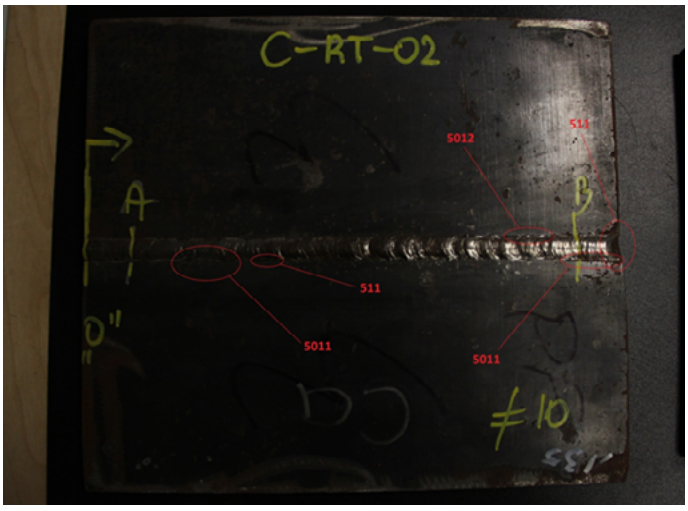

Fig 4. Exemplary external imperfections detected on the weld face surface: 5011 – continuous undercut, 5012 – intermittent undercut and 511 – incompletely filled groove; the yellow colour marks the testing direction and the location of the zero point (in relation to which the location of individual discontinuities is determined)

Radiographic test

The radiographic test involved the calibration of the detector system followed by the attachment of a copper filter (t = 2 mm), the connection of power supply, the identification of exposure parameters (Table 7) and the analysis of the joint. The test was 12 minutes in duration. The radiogram (Fig. 5) obtained in the test was subjected to assessment aimed to determine the location and the size of discontinuities. The test results are presented in Table 8.

Table 7. Test parameters

Parameter	Value
Voltage, kV	180
Current, mA	5
Number of integrations	5
Sensitivity level	4pF

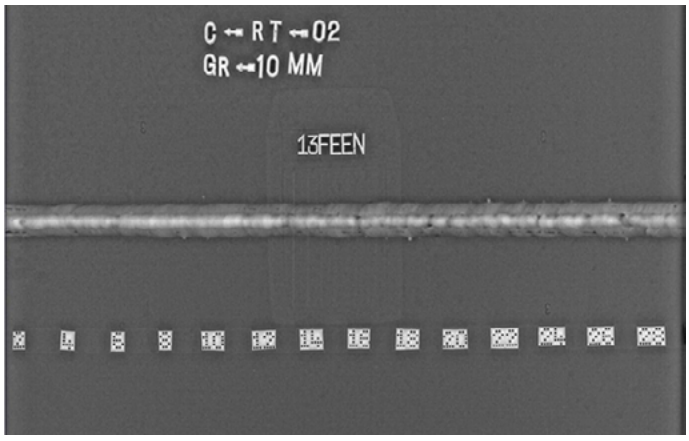

Fig. 5. Radiogram of the joint subjected to tests – incomplete fusions were detected along nearly the entire length. It should be noted that the weld was turned horizontally by 180°. Therefore, in the above-presented image, the previously determined zero point is located on the right.

Table 8. Radiographic test results

No.	Type of discontinuity (reference number)	Distance to the zero point, mm	Length of discontinuity, mm	Distance to the weld axis [1], mm
1.	Surface pore (2017)	4.27	1.75	-5.2
2.	Undercut (501)	21.82	2.52	-1.97
3.	Lack of side-wall fusion (4011)	27.48	18.72	4.71
4.	Lack of side-wall fusion (4011)	54.96	29.98	5.36
5.	Continuous undercut (5011)	63.39	1.31	-0.66
6.	Lack of side-wall fusion (4011)	97.55	5.04	4.71
7.	Surface pore (2017)	107.19	0.66	5.04
8.	Continuous undercut (5011)	110.69	2.74	1.97
9.	Lack of side-wall fusion (4011)	114.85	16.2	5.15
10.	Lack of side-wall fusion (4011)	142.33	28.36	4.27
11.	Continuous undercut (5011)	143.32	2.19	-1.75
12.	Lack of side-wall fusion (4011)	161.28	3.39	-5.26
13.	Gas pore (2011)	179.01	1.53	-5.47
14.	Lack of side-wall fusion (4011)	189.53	4.82	-5.58
15.	Undercut (501)	208.46	2.13	-3.08
16.	Lack of side-wall fusion (4011)	223.13	2.1	3.86
17.	Continuous undercut (5011)	248.65	2.24	-2.14
18.	Surface pore (2017)	267.37	1.48	3.5
19.	Continuous undercut (5011)	290.47	10.51	4.51
20.	Continuous undercut (5011)	291.35	9.2	-5.2
21.	Incompletely filled groove (511)	297.81	2.19	-

1) Discontinuities were located on both sides of the joint, therefore the negative values refer to the imperfections located on the right side of the weld axis (in relation to the zero point).

Phased-Array Ultrasonic Test

The performance of the ultrasonic tests required the appropriate preparation of the test rig and the calibration of the equipment. Because of the scanner design (i.e. its arms being located at a certain distance from its main axis), the area subjected to examination was extended by the so-called "run-out", i.e. a longer distance covered by the machine wheels (Fig. 6).

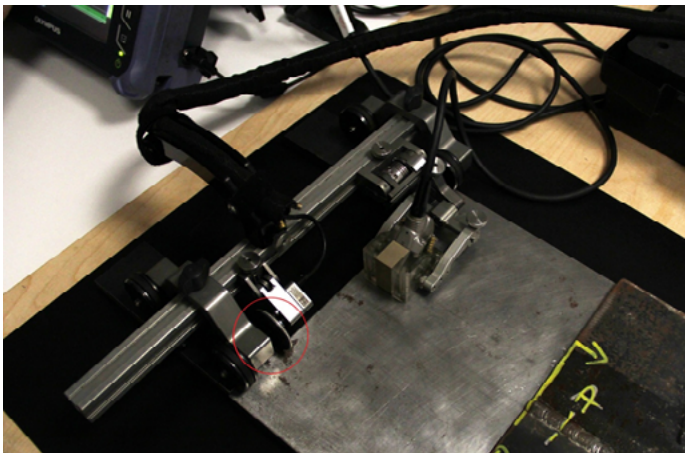

Fig 6. Standard master-based calibration process: run-out plates are located under the scanner wheels; the encoder is marked with the red colour

After calibration, the transducer was placed on the surface of the test joint. Next, it was necessary to determine the position of the scanner in relation to the weld and cover the element with a small amount of demineralised water (i.e. the medium of acoustic feedback). The test was performed in two directions, i.e. 90° and 270°, in relation to the plane of the weld axis. As a result, it was possible to obtain the image of the entire joint area. The test (being 3 minutes in duration) was followed by measurements and the assessment of indications.

The parameters used in the test are presented in Table 9, whereas the results of the test are

presented in Table 10. Figures 7 and 8 present defectoscope screenshots.

Table 9. Parameters used in the PAUT process

Parameter	Value
Voltage, V	40
Gain, dB	21.52
Transducer impulse frequency, MHz	5
Digitalisation frequency, MHz	100
Maximum acquisition rate, mm/s	60
Beam angular range, °	40–70
Impulse width, ns	100

TOFD test

Preparations preceding the time of flight diffraction test (TOFD) were similar to those preceding the phased-array ultrasonic test. The test (being 2 minutes in duration) involved both the face and the root of the weld. The parameters

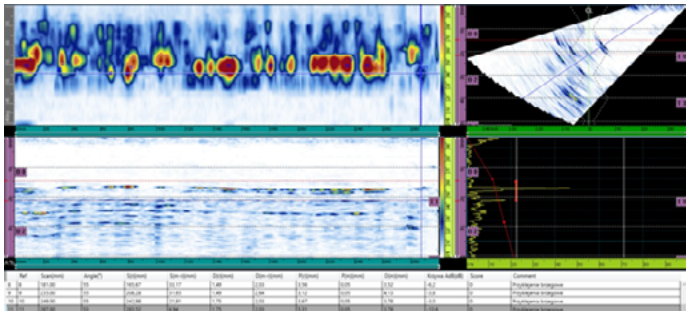

Fig. 7. Indications obtained during the test 270°-oriented tests

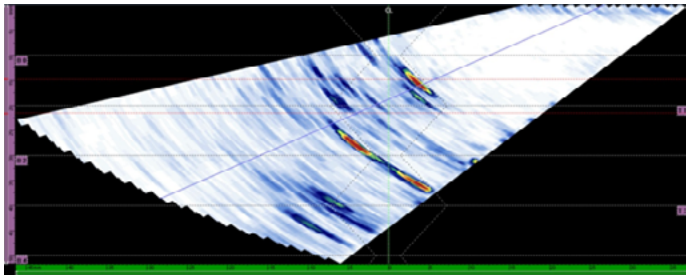

Fig. 8. S-scan (270° test) with a very clear indication; location near the bevelled wall implies incomplete fusion. The obtainment of the above-presented image is connected with the phenomenon of diffraction on the surface of an imperfection (highly desirable during PA tests)

Table 10. Phased-array ultrasonic test results

No.	Type of discontinuity (reference number)	Distance to the zero point, mm	Length, mm	Depth, mm	Height, mm	Position in relation to the weld axis[1)], mm
1.	Porosity (2013)	0.45	6.06	0.01	5.27	-3.54
2.	Lack of side-wall fusion (4011)	1.11	20.09	1.84	2.47	3.72
3.	Lack of side-wall fusion (4011)	1.66	17.7	1.32	2.55	-5.06
4.	Lack of side-wall fusion (4011)	29.02	14	2.81	1.85	5.09
5.	Lack of side-wall fusion (4011)	62.8	7.91	2.81	1.85	5.09
6.	Lack of side-wall fusion (4011)	62.8	7.94	2.55	1.67	5.8
7.	Lack of side-wall fusion (4011)	74.55	12.23	1.93	2.73	6.29
8.	Lack of side-wall fusion (4011)	100.24	5.48	2.9	1.5	5.41
9.	Lack of side-wall fusion (4011)	106.81	19.81	2.28	2.64	-5.12
10.	Lack of side-wall fusion (4011)	123.07	38.35	1.14	2.47	4.32
11.	Lack of side-wall fusion (4011)	136.02	7.52	2.11	2.91	-4.96
12.	Lack of side-wall fusion (4011)	165.67	33.17	1.49	2.04	3.56
13.	Lack of side-wall fusion (4011)	166.54	13.04	2.46	1.94	-3.97
14.	Undercut (501)	203.63	1.88	0.01	1.39	-5.45
15.	Lack of side-wall fusion (4011)	208.28	31.65	1.49	2.64	3.12
16.	Lack of side-wall fusion (4011)	230.64	2.76	0.08	2.82	-4.03
17.	Lack of side-wall fusion (4011)	242.98	21.91	1.75	2.03	3.67
18.	Lack of side-wall fusion (4011)	263.68	5.76	1.67	1.94	-3.32
19.	Lack of side-wall fusion (4011)	283.52	6.94	1.75	2.03	3.67
20.	Lack of side-wall fusion (4011)	288.73	3.88	1.67	1.67	-3.65

1) Negative values refer to imperfections located on the right side of the weld axis (in relation to the zero point)

used in the test are presented in Table 11, whereas the results of the test are presented in Table 12. Figures no. 9 and 10 present defectoscope screenshots.

Table 11. Parameters used in the TOFD tests

Parameter	Value
Voltage, V	175
Gain, dB	77 (root), 81 (face)
Transducer impulse frequency, MHz	15
Digitalisation frequency, MHz	100
Maximum acquisition rate, mm/s	60
Impulse width, ns	32,5
Beam angle of incidence, °	70

Metallographic tests

The determination of indication accuracy required the performance of metallographic tests enabling the actual measurement of identified discontinuities. To this end, the specimen was cut up into 18 pieces (Fig. 11) and subjected to visual tests involving the use of a microscope and a 20-fold magnification. The results of the test are presented in Figure 12.

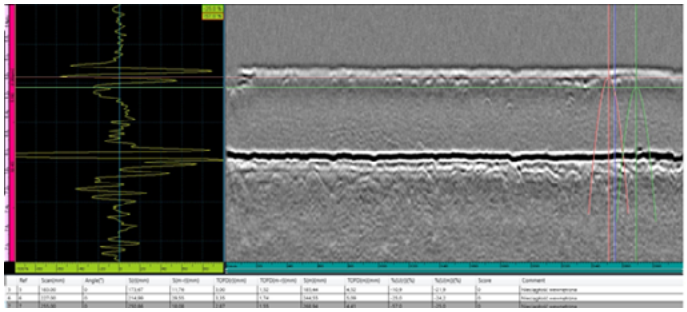

Fig.9. Defectoscopic image in the weld face test: A-scan (left) and B-scan (right)

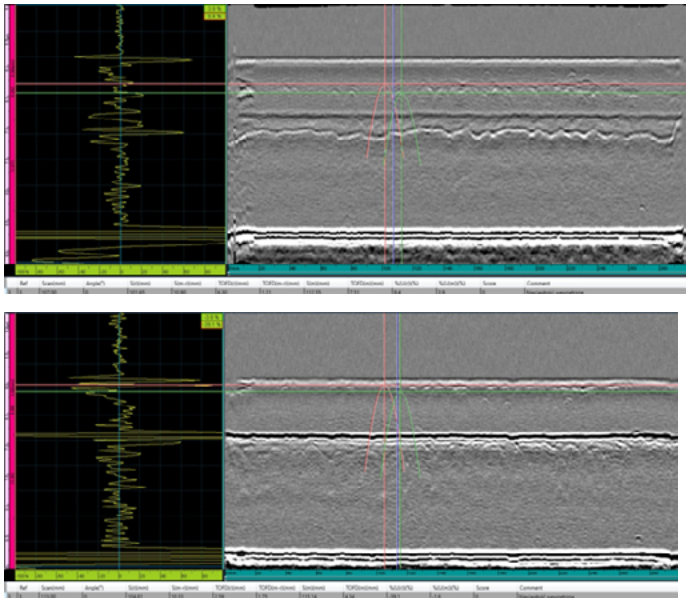

Fig. 10. Image of the same discontinuity from the weld face side (top) and the weld root side (bottom)

Table 12. Results obtained in the TOFD tests

No.	Type of discontinuity [1)]	Distance to the zero point, mm	Length, mm	Depth, mm	Height, mm
1.	Weld face surface-breaking discontinuity	0.41	17.84	2.45	1.9
2.	Internal discontinuity	70.09	14.63	2.73	1.52
3.	Internal discontinuity	104.81	10.33	2.95	1.75
4.	Internal discontinuity	121.74	37.02	2.59	2.01
5.	Internal discontinuity	173.67	11.76	3.00	1.52
6.	Internal discontinuity	214.99	29.55	3.35	1.74
7.	Internal discontinuity	250.86	18.08	2.87	1.55
8.	Point-like indication in the weld root	270.37	3.44	9.58	0.48

1) Because of the impossibility of locating discontinuities in the y-axis (perpendicular to the weld axis), the identification of the types imperfections was impeded. Because of this, in the TOFD technique, the description of imperfections is usually limited to the location of the imperfection in the joint.

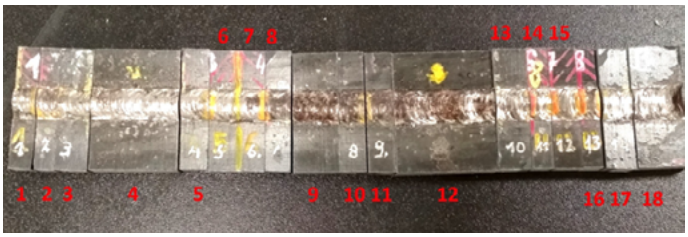

Fig. 11. Marking of the specimens (red numerals apply; engraved numbering was only used during grinding)

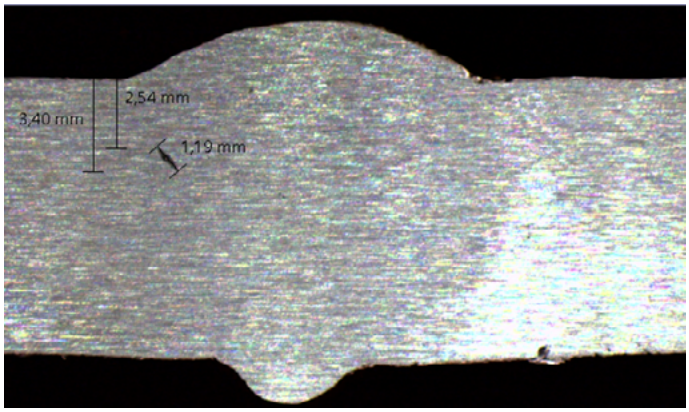

Fig. 12. Image of the right side of specimen 12

Table 13. Results of macroscopic metallographic tests

Specimen designation[1)]	Type of discontinuity (reference number)	Distance to the zero point, mm	Depth, mm	Height, mm	Location in relation to the weld axis[2)], mm
P1-P	Lack of side-wall fusion (4011) Gas pore (2011) Lack of side-wall fusion (4011)	10	2.69 1.9 2.05	1.95 1.31 1.13	5.57 4.59 -4.91
P2-L	Lack of side-wall fusion (4011) Lack of side-wall fusion (4011) Gas pore (2011)	12	2.02 2.4 5.53	1.15 1.7 0.35	4.33 -4.4 4.79
P3-P	Lack of side-wall fusion (4011)	70	2.4	0.76	5.12
P5-L	Gas pore (2011)	72	0.99	0.08	1.13
P7-P	Lack of side-wall fusion (4011)	107	2.72	1.04	-4.05
P8-L	Lack of side-wall fusion (4011)	109	2.3	1.07	4.82
P9-L	Lack of side-wall fusion (4011) Lack of side-wall fusion (4011)	121	2.62 2.54	0.83 0.78	-4.73 4.58
P9-P	Lack of side-wall fusion (4011)	140	1.81	1.13	5.04
P10-L	Lack of side-wall fusion (4011)	142	3.41	0.23	-4.03
P10-P	Lack of side-wall fusion (4011)	152	2.43	0.81	-4.5
P11-L	Undercut of a weld root (5013) Lack of side-wall fusion (4011)	154	9.58 2.72	0.42 1.91	1.98 -4.41
P11-P	Lack of side-wall fusion (4011)	165	2.38	0.89	3.96
P13-L	Lack of side-wall fusion (4011)	209	3	1.79	-3.8
P13-P	Lack of side-wall fusion (4011)	222	2.57	1.2	-5.02
P14-L	Lack of side-wall fusion (4011)	224	2.77	0.98	-4.26
P14-P	Lack of side-wall fusion (4011)	233	2.14	1.55	-5.41
P15-L	Lack of side-wall fusion (4011)	235	2.42	0.76	-5.87
P15-P	Lack of side-wall fusion (4011)	246	2.54	1.19	-5.56
P16-L	Lack of side-wall fusion (4011)	248	2.33	1.28	-5.89
P17-L	Lack of side-wall fusion (4011) Lack of side-wall fusion (4011)	258	1.51 2.11	1.21 0.74	4.72 -5.68

1) The letter "P" refers to the right side of the specimen (in relation to the start of an area subjected to the test), whereas the letter "L" – refers to the left side of the specimen
2) Discontinuities were located on both sides of the joint, therefore the negative values refer to imperfections located on the right side of the weld axis (in relation to the zero point).

Analysis of results

Among the techniques used in the tests, only the radiographic method enabled the detection of external imperfections from groups II and IV. The aforesaid imperfections were located on the weld face surface or open on the side of the weld face. The list of the imperfections is presented in Table 14.

In relation to all detected external discontinuities from groups II (cavities) and IV (incomplete fusion and the lack of penetration), the efficacy of the individual methods was as follows:

– RT – 11 indications,
– UT - PA – 2 indications,
– UT - TOFD – 1 indication.

Table 15 presents the comparison of the measurement results obtained during the TOFD tests with those obtained during the metallographic test. Table 16 presents the comparison of the measurement results obtained in the phased-array ultrasonic tests (PAUT) with those obtained during the metallographic test.

The analysis of data presented in Tables 15 and 16 revealed that, in most cases, the TOFD enabled the significantly more precise identification of the height and the depth of the defects. An exception was item no. 3, where the difference in height measurements amounted to more than 142%. The foregoing resulted from the excessive value of adjusted gain, which led to image deformation and the misinterpretation of the A-scan.

An interesting case could be observed in relation to item no. 3 (concerning the comparison of the PAUT method), where the depth was identified with a very small difference. The reason for such a result was the presence of a diffraction echo, where the emitted wave struck the surface of the defect at an angle of 90°, thus enabling the obtainment of a very accurate indication. Such phenomena are highly desired in the tests as they eliminate the primary limitation of the PA technique (i.e. uncertainty concerning measurements of the depth and the height of discontinuities), yet their obtainment is extremely problematic.

The measurement of the location in relation to the weld axis was performed using the RT method and the PAUT method. In terms of the TOFD technique, the performance of the aforesaid measurement is impossible). The results are presented in Tables 17 and 18.

In most of the above-presented cases, the PAUT method enabled the significantly more accurate determination of the defect location in the y-axis (perpendicular to the weld axis) than the radiographic method.

Table 14. Comparison of indications of external imperfections on the weld face side

No.	RT		PAUT		TOFD	
	Type	Distance, mm	Type	Distance, mm	Type	Distance, mm
1.	Surface pore	4.27	Porosity	0.45	Open	0.41
2.	Undercut	26.82	Undercut	203.63	Not detected	-
3.	Continuous undercut	63.39	Not detected	-	Not detected	-
4.	Surface pore	107.19	Not detected	-	Not detected	-
5.	Continuous undercut	110.69	Not detected	-	Not detected	-
6.	Continuous undercut	143.32	Not detected	-	Not detected	-
7.	Undercut	208.46	Not detected	-	Not detected	-
8.	Surface pore	267.37	Not detected	-	Not detected	-
9.	Continuous undercut	290.47	Not detected	-	Not detected	-
10.	Continuous undercut	291.35	Not detected	-	Not detected	-
11.	Incompletely filled groove	297.81	Not detected	-	Not detected	-

Table 15. Comparison of measurements of selected indications (metallographic tests and TOFD)

No.	Metallographic test			TOFD			Difference in relation to	
	Distance, mm	Depth, mm	Height, mm	Distance, mm	Depth, mm	Height, mm	depth, %	height, %
1.	70	2.4	0.76	70.09	2.73	1.52	**13.8**	**100**
2.	107	2.72	1.04	104.81	2.95	1.75	**8.5**	**68.3**
3.	121	2.62	0.83	121.74	2.59	2.01	**1.1**	**142.2**
4.	248	2.33	1.28	250.86	2.87	1.55	**23**	**21.1**

Table 16. Comparison of measurements of selected indications (metallographic tests and PAUT)

No.	Metallographic test			TOFD			Difference in relation to	
	Distance, mm	Depth, mm	Height, mm	Distance, mm	Depth, mm	Height, mm	Distance, mm	Depth, mm (s12)
1.	107	2.72	1.04	106.81	2.28	2.64	**16.2**	**153.8**
2.	121	2.62	0.83	123.07	1.14	2.47	**56.5**	**197.6**
3.	165	2.38	0.89	166.54	2.46	1.94	**3**	**118**
4.	209	3	1.79	208.28	1.49	2.64	**101.3**	**47.5**

Table 17. Comparison of measurements of selected indications (metallographic tests and PAUT)

No.	Metallographic test		PAUT			Difference of location, %
	Distance, mm	Location in relation to the weld axis, mm	Distance, mm	Length, mm	Location in relation to the weld axis, mm	
1.	107	-4.05	106.81	19.81	-5.12	**26.4**
2.	121	4.58	123.07	38.35	4.32	**5.7**
3.	142	-4.03	136.02	7.52	-4.96	**23.1**
4.	165	3.96	165.67	33.17	3.56	**10.1**

Table 18. Comparison of measurements of selected indications (metallographic tests and RT)

No.	Metallographic test		PAUT			Difference of location, %
	Distance, mm	Location in relation to the weld axis, mm	Distance, mm	Length, mm	Location in relation to the weld axis, mm	
1.	107	-4.05	107.19	0.66	5.04	**224.4**
2.	121	4.58	114.85	16.2	5.15	**12.4**
3.	142	-4.03	143.32	2.19	-1.75	**56.3**
4.	165	3.96	142.33	28.36	4.27	**7.8**

Attention should be paid to item no. 1 in Table 18, where both indications have different (opposite) signs, indicating locations on the opposite sides of the weld. The foregoing could imply the wrong reading of the radiogram.

Concluding remarks

The analysis of the results of the above-presented tests justified the formulation of the following conclusions:

1. In most cases, the TOFD technique enabled the significantly more precise identification

of the height of a given imperfection as well as the determination of its actual location in the z-axis (depth). In turn, the identification of the location in relation to the weld axis required the application of the PAUT method.

2. In relation to selected imperfections, the PAUT method enabled the obtainment of results significantly more similar to the metallographic test results than the radiographic method.

Further tests

The above-presented results demonstrate the efficacy of ultrasonic tests when examining butt welded joints made of boiler steel. However, the above-presented range is still overly narrow to identify the industrial usability of the tests. For this reason, further research should focus on the identification of parameters enabling the optimisation of the process. Particularly interesting are obtainable scanning rates and the reduction of test duration, i.e. the issues raised by the transport industry (e.g. tests of welded joints in railway rails). Another important aspect is concerned with materials (e.g. aluminium), the properties of which could adversely affect the propagation of waves deep inside an element being tested. The analysis of such issues, supported by appropriate results, could enable the satisfaction of requirements formulated by industrial partners and the practical application of developed solutions.

References

[1] Praca zbiorowa: Poradnik inżyniera. Spawalnictwo. Tom 1, Wydawnictwa Naukowo-Techniczne, Warszawa 2003.
[2] Chaplin R.: Industrial Ultrasonic Inspection: Levels 1 and 2, FriesenPress, Altona 2017.
[3] Schmerr Jr., Lester W.: Fundamentals of Ultrasonic Nondestructive Evaluation: A Modeling Approach, Springer, 2018.
[4] Czuchryj J., Sikora S.: Niezgodności spawalnicze w złączach spawanych z metali i termoplastycznych tworzyw sztucznych. Instytut Spawalnictwa, Gliwice 2016.
[5] [Online] https://www.polmet.eu/blog/charakterystyka-stali-p265gh (access date: 21.12.2020).
[6] [Online]http://www.mistal.pl/2013-03-26-17-30-34/rury-do-zastosowan-cisnieniowych-w-podwyzszonych-temperaturach-rury-kotlowe-pn-en10216-2-din-17175 (access date: 21.12.2020).
[7] [Online]https://www.rywal.com.pl/produkty/urz%C4%85dzenia-spawalnicze-i-zgrzewarki/origo-mig-430w-esab-spawarka-detail.html (access date: 29.12.2020).
[8] [Online]http://www.nortechweld.pl/produkty?format=raw&task=download&fid=111(access date: 28.12.2020).
[9] [Online]https://www.ti-ba.com/wp-content/uploads/2014/03/TI-BA-XRD-4336-DR.pdf (access date: 29.12.2020).
[10] [Online]https://www.bakerhughesds.com/sites/g/files/cozyhq596/files/acquiadam_assets/eresco_65_mf4_air-cooled_brochure_deutsch.pdf (access date: 29.12.2020).
[11] [Online] https://www.olympus-ims.com/pl/omniscan-sx/ (access date: 30.12.2020).
[12] [Online]https://www.olympus-ims.com/pl/hst-lite (access date: 30.12.2020).